Chinese Chemical Letters 36 (2025) 109640

Contents lists available at ScienceDirect

Chinese Chemical Letters

journal homepage: www.elsevier.com/locate/cclet

Investigation on Cu promotion effect on Ce-based solid solution-anchored Rh single atoms for three-way catalysis

Jianing He[a,b], Xiao Wang[a,b,*], Zijian Wang[a,b], Ruize Jiang[a,b], Ke Wang[a,b], Rui Zhang[a,b], Huilin Wang[a,b,*], Baokang Geng[a,b], Hongyi Gao[c], Shuyan Song[a,b,*], Hongjie Zhang[a,b,d]

[a] State Key Laboratory of Rare Earth Resource Utilization, Changchun Institute of Applied Chemistry, Chinese Academy of Sciences, Changchun 130022, China
[b] School of Applied Chemistry and Engineering, University of Science and Technology of China, Hefei 230026, China
[c] China School of Materials Science and Engineering, University of Science and Technology Beijing, Beijing 100083, China
[d] Department of Chemistry, Tsinghua University, Beijing 100084, China

ARTICLE INFO

Article history:
Received 14 December 2023
Revised 30 January 2024
Accepted 7 February 2024
Available online 10 February 2024

Keywords:
Three-way catalysts (TWC)
Solid solution
Co-precipitation
Rhodium (Rh) catalyst
Oxygen vacancies

ABSTRACT

The three-way catalyst (TWC), as a promising approach to control automobile exhaust emission, has been widely studied and applied. However, it still suffers from the high light-off temperature and poor stability. Herein, we synthesized a multicomponent catalyst Rh/Cu-CeSn by using Cu metal doping to modify the Ce-based solid solution, which exhibited good TWC catalytic performance: the light-off temperatures for CO, NO, and C_3H_6 conversion are 172 °C, 266 °C, and 193 °C, respectively. Moreover, the catalyst still maintained good activity after 12 h of the continuous reaction under high-temperature conditions. The experiments and mechanism studies reveal that due to the redox pair Cu^+/Cu^{2+}, the Cu incorporation can effectively inhibit the Rh transition to the oxidation state and greatly enhance the catalytic activity and stability. This work provides a viable strategy for precise characteristic modulation of composite oxide supports during the fabrication of noble metal-based catalysts, which significantly reduces environmental pollution from energy applications.

Severe automobile exhaust emissions, one of the air pollutants, have caused a great threat to human health and world environment, attracting widespread attention [1–3]. As a promising technique to improve air quality, the three-way catalysts (TWCs) have been deeply studied and applied, since they can convert the three pollutants carbon monoxide (CO), nitrogen monoxide (NO), and hydrocarbons (HCs) from automobile exhaust into non-toxic carbon dioxide (CO_2), nitrogen (N_2), and H_2O effectively and simultaneously [4]. However, although considerable efforts have been made, developing high-performance TWCs with low-temperature activity and high-temperature stability while reducing the cost remains challenging [5,6].

In recent years, Ce-based solid solutions have been widely used as catalyst supports for various catalytic reactions, due to their unique oxygen storage capacity and excellent redox properties [7,8]. Previous reports have pointed out that the incorporation of foreign metal atoms (such as Zr, Sn, Ti, Mn) into the CeO_2 lattice to construct Ce-based solid solution leads to changes in crystallite size and lattice strain, which is beneficial to the formation of more oxygen vacancies and the activation of reactant molecules, greatly promoting the catalytic performance enhancement [9–12]. Safonova and co-workers [13] have shown that the easier reducibility of Ce^{4+} at the $Pt/Ce_{0.5}Sn_{0.5}O_2$ interface increases the catalytic CO oxidation rate, owing to the two electrons exchange between Ce^{4+}/Ce^{3+} and Sn^{4+}/Sn^{2+} redox couples through the redox equilibrium of $2Ce^{3+} + Sn^{4+} \leftrightarrow 2Ce^{4+} + Sn^{2+}$. Although many advances have been made in CeSn-based solid solutions so far, due to the lack of an in-depth study of the structure-activity relationship at the interface, there is still much interest in improving their three-way catalytic performances which are important for practical catalytic applications [14–17].

Herein, we synthesize a series of high-performance Rh/Cu-CeSn catalysts for efficient TWC reaction by introducing the Cu atoms to CeSn-based solid solutions. Experiments and mechanism studies have confirmed that the presence of Cu^+ and Cu^{2+} ions can not only increase the amount of support oxygen vacancy but also effectively inhibit Rh from being oxidized. Compared to the bare Rh/CeSn, the Rh/Cu-CeSn catalyst shows higher TWC catalytic activity and stability: Its T_{50} values for CO, NO, and C_3H_6 conversion are 172 °C, 266 °C, and 193 °C, respectively, and over 95% of the

* Corresponding authors.
E-mail addresses: wangxiao@ciac.ac.cn (X. Wang), wanghl@ciac.ac.cn (H. Wang), songsy@ciac.ac.cn (S. Song).

https://doi.org/10.1016/j.cclet.2024.109640
1001-8417/

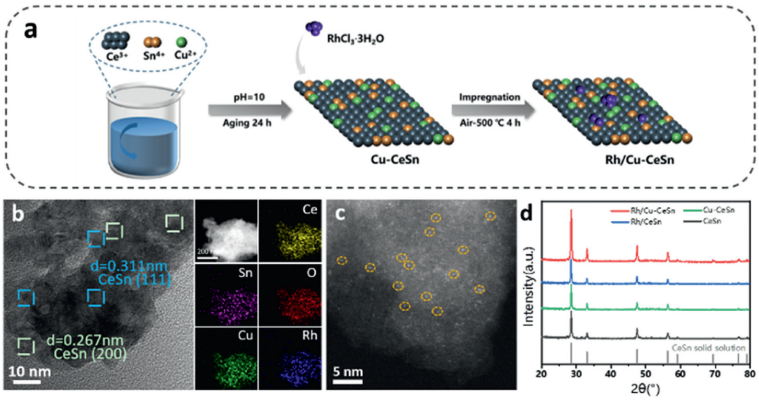

Fig. 1. (a) The synthesis route of Rh/Cu-CeSn. (b) TEM image of Rh/Cu-CeSn and the corresponding EDX mapping images. (c) HAADF-STEM image of Rh/Cu-CeSn with the Rh SAs highlighted by the orange circles. (d) XRD patterns of the Rh/Cu-CeSn, Rh/CeSn, Cu-CeSn and CeSn.

initial activity can remain after 12 h constantly operating at 400 °C, greatly improving the catalytic performance.

The specific synthesis route of the Rh/Cu-CeSn catalyst is shown in Fig. 1a. The CeSn solid solution modified by Cu (Cu-CeSn) was first prepared by the co-precipitation method. Because of the crystal structure similarity of Cu with Ce and Sn, and its beneficial effect on inducing charge defect generation and valence state change, Cu can be easily incorporated into CeSn solid solution as dopant [18,19]. Then, the Rh/Cu-CeSn was obtained by the impregnation method, in which the loading of Rh was controlled at 0.8 wt%, and detailed results of inductively coupled plasma optical emission spectrometry (ICP-OES) are shown in Table S1 (Supporting information). Scanning electron microscopy (SEM) and transmission electron microscopy (TEM) were carried out to observe the morphology of the catalysts. The SEM and TEM images reveal that the Rh/Cu-CeSn catalyst is composed of small nanoparticles, and the lattice distance of 0.311 nm and 0.267 nm measured from the TEM image matches well with the (111) and (200) planes of CeSn solid solution (Fig. 1b, Figs. S1 and S2 in Supporting information). The corresponding energy-dispersive X-ray spectroscopy (EDX) mapping images show that the Ce, Sn, Cu, Rh, and O elements are dispersed homogeneously. The high-angle annular dark-field scanning transmission electron microscopy (HAADF-STEM) was further performed to determine the fine structure of the catalyst. The STEM image in Fig. 1c shows clearly that the visible single-atom Rh disperses on the Cu-CeSn support. Besides, X-ray diffraction (XRD) was used to determine the composition of the obtained catalysts. The XRD patterns of all catalysts only exhibit diffraction peaks at 28.55°, 33.08°, 47.48°, and 56.34°, in line with the CeSn solid solution (111), (200), (220), and (311) characteristics planes, respectively (Fig. 1d). No diffraction peaks relating to Cu or Rh are observed, indicating that these two metals are highly dispersed. The specific surface area of the catalysts was also determined by nitrogen adsorption-desorption, in which the Brunauer-Emmett-Teller (BET) specific surface area of Rh/Cu-CeSn was 51.297 m^2/g, similar to that of Cu-CeSn support and CeSn solid solution, reflecting that Rh loading and Cu doping do not significantly change the morphology and the surface area of the catalysts (Fig. S3 and Table S2 in Supporting information). The above results prove that the successful formation of the Rh/Cu-CeSn solid solution catalyst [11].

Next, to explore the redox properties in-depth, the reduction behavior of four catalysts was measured by temperature-programmed reduction of hydrogen (H_2-TPR), and the profiles are shown in Fig. 2a. Two clear reduction peaks at around 500 °C and 750 °C are observed, which are identical with these of pure CeO_2. The low-temperature peak is attributed to the reduction of surface CeO_2, and the high-temperature peak belongs to the reduction

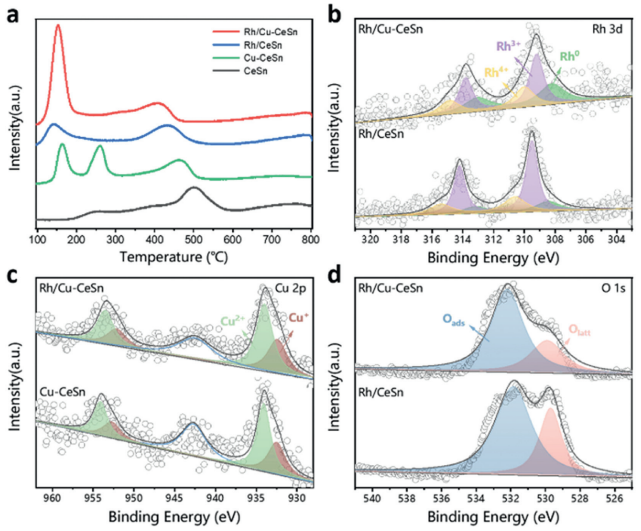

Fig. 2. (a) H_2-TPR profiles of the Rh/Cu-CeSn, Rh/CeSn, Cu-CeSn and CeSn. (b) XPS spectra of Rh 3d and (d) O 1s over the Rh/Cu-CeSn, Rh/CeSn. (c) XPS spectra of Cu 2p over the Rh/Cu-CeSn, Cu-CeSn.

of volume CeO_2 [20–22]. For Rh/Cu-CeSn and Rh/CeSn, Cu-CeSn and CeSn, the two reduction peaks shift to the low-temperature direction obviously with the addition of Cu, which results from the strong interaction between Ce^{4+}/Ce^{3+} and Sn^{4+}/Sn^{2+} in the presence of Cu through the redox equilibrium of $2Ce^{3+} + Sn^{4+} \leftrightarrow 2Ce^{4+} + Sn^{2+}$, indicating that the oxygen atoms of the Rh/Cu-CeSn catalyst are more easily transferred and produce oxygen vacancies during the reduction process [23]. In addition, for the Cu-CeSn support, the peak near 160 °C can be attributed to the reduction of finely dispersed Cu^{2+} species to Cu^+ by strong interaction with the support, and the peak around 260 °C corresponds to the reduction of larger CuO particles on the surface of the solid solution [24–26]. Notably, by comparing Rh/Cu-CeSn with Cu-CeSn, the Rh species plays a key role in increasing the dispersity of Cu species and promoting its reduction. And the reduction peak centered around 150 °C can be attributed to the reduction of RhO_x species, which is located on the support and the interface between metals and supports [27,28]. It has been reported that there may be a spillover effect between the noble metal active component and the easily reduced Ce-based support, resulting in the partial reduction of Ce^{4+} on the support surface and slight oxidation of the active component Rh [29,30].

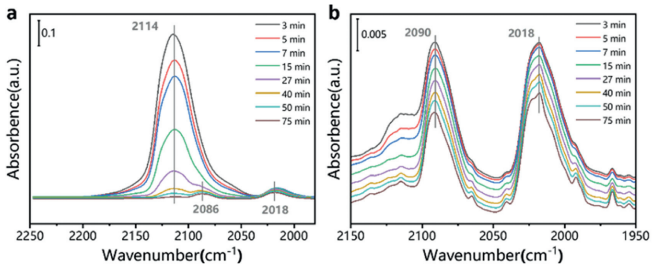

Fig. 3. The evolution of CO adsorption spectra of the (a) Rh/Cu-CeSn and (b) Rh/CeSn after 30 min purged with pure He (50 mL/min) at 200 °C, and then adsorbed CO for 20 min to saturation.

The surface chemistry changes and electronic states of the catalysts were further investigated by X-ray photoelectron spectroscopy (XPS). The Rh 3d, Cu 2p, and O 1s XPS spectra of different catalysts are shown in Fig. 2 and Fig. S4 (Supporting information), and the relative proportions of different species of these elements are summarized in Table S3 (Supporting information). The Rh 3d XPS spectra of Rh/Cu-CeSn and Rh/CeSn are both fitted with six peaks assigned to three pairs of spin-orbit doublets (Fig. 2b). Specifically, the Rh $3d_{5/2}$ peaks at 307.3, 309.0, and 310.6 eV could be assigned as Rh^0, Rh^{3+}, and Rh^{4+}, respectively. Previous studies have proved that Rh^0 and Rh^{3+} species are catalytically active species for three-way catalytic reactions due to their good redox properties, while Rh^{4+} species is less active because it is more difficult to reduce [31,32]. Comparing Rh/Cu-CeSn with Rh/CeSn, the addition of Cu induces the binding energy of Rh species (Rh^0 and Rh^{3+}) to decrease significantly, resulting in a distinct increase of the electron cloud density, which contributes to maintaining Rh species at a low valence state. The proportion of Rh^0 over Rh/Cu-CeSn is calculated to be 31.95%, which is much higher than that over Rh/CeSn (16.51%, Table S3). The Cu 2p spectra of Rh/Cu-CeSn and Cu-CeSn show that the Cu $2p_{3/2}$ photopeak centered at 934.0 eV is accompanied by a shake-up satellite structure in the range 939~947 eV which embodies the presence of the Cu^{2+} species, while the peak band near 932.5 eV is ascribed to the Cu^+ species (Fig. 2c) [33]. And the relative proportions of Cu species represent that there is a high proportion of Cu^{2+} in the Rh/Cu-CeSn catalyst because the redox pair of Cu affects the Rh transition between different species, preventing the oxidation of Rh metal (Table S3). The O 1s spectra of four catalysts (Fig. 2d and Fig. S4) depict that these peaks are asymmetric, indicating two different O chemical species exist in the catalysts. The peak at low binding energies (529.8–530.1 eV) labeled as O_{latt} is attributed to the association with the lattice oxygen of metal oxides, and the other peak at high binding energies (531.3–533.3 eV) denoted as O_{ads} is the characteristic of surface-adsorbed oxygen and oxygen vacancy which are related to surface-active oxygen species [34,35]. The relative proportions of O species listed in Table S3 represent the concentration of oxygen vacancies. Comparing these four catalysts, the Rh/Cu-CeSn catalyst has the highest oxygen vacancy concentration (72.4%) and the Cu addition significantly increases the oxygen vacancies of the catalyst.

Then, the Rh/Cu-CeSn and Rh/CeSn catalysts were characterized by *in situ* CO-diffuse reflectance infrared Fourier transform spectroscopy (CO−DRIFTs), in order to explore the interaction between Cu and Rh [36]. The catalysts are purged with pure He (50 mL/min) at 200 °C for 30 min to completely remove adsorbed species on the catalyst surface. Subsequently, the CO is introduced for 20 min to ensure CO adsorption onto the active sites, and the evolution of CO adsorption spectra are shown in Fig. 3. The two adsorption peaks at ~2088 and ~2018 cm^{-1} correspond to the CO on Rh single atoms and they are attributed to the symmetric and asymmetric CO-stretching mode of $Rh(CO)_2$ species in accordance with previous studies, which agrees with our HAADT-STEM results [37,38]. In addition, a strong adsorption peak at ~2114 cm^{-1} is also observed, which can be assigned to the linear CO adsorbed on Cu^+ sites (Cu^+-CO), and it can also be detected in the Cu-CeSn support (Fig. S5 in Supporting information) [39]. This validates the successful doping of the Cu metal and its high dispersion in the catalysts, consistent with our XPS and TPR results. And the strong adsorption peak suggests that there is a certain amount of Cu^+ species in the Rh/Cu-CeSn and Cu-CeSn catalysts at low temperatures, and they would have a strong ability to adsorb CO at low temperatures [40].

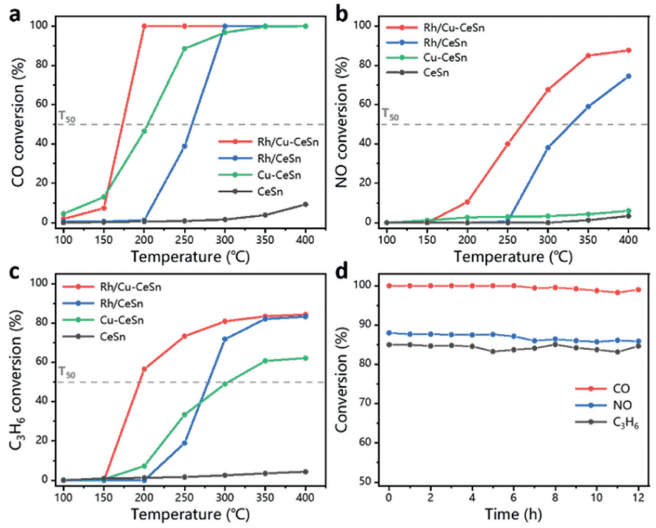

Fig. 4. (a) CO oxidation, (b) NO reduction, and (c) C_3H_6 oxidation by the Rh/Cu-CeSn, Rh/CeSn, Cu-CeSn, CeSn. (d) The stability TWC test by the Rh/Cu-CeSn. The space velocity was set at 200,000 mL g^{-1} h^{-1}. The feed gas is composed of 2% CO, 1.75% O_2, 2000 ppm C_3H_6, 500 ppm NO, balance Ar.

To deeply study the influence of Cu on the three-way catalytic performance of the Rh-supported CeSn solid solution catalyst, the three-way catalytic performance of different catalysts was measured by the fix-bed reactor under a weight hourly space velocity of 200,000 mL g^{-1} h^{-1}. The conversion curves of CO, NO, and C_3H_6 for different catalysts are shown in Fig. 4 and the T_{50} (the reaction temperature required when the conversion rate reaches 50%) values are listed in Table S4 (Supporting information). The pure support CeSn has almost no catalytic activity in the range of test temperature, and the Rh/CeSn has certain activity, which its T_{50} values for CO, NO, and C_3H_6 conversion are 258 °C, 329 °C, and 282 °C, respectively. After the modification of Cu, the three-way catalytic performance of the Rh/Cu-CeSn catalyst has been prominently increased, and the light-off temperatures of CO, NO, and C_3H_6 decreased by 86 °C, 63 °C, and 89 °C, respectively. To confirm the role of Cu species, we also prepared the Cu-CeSn support and tested its TWC performance (Fig. S6 in Supporting information). It can be found that the Cu-CeSn support has good CO oxidation activity, as the previous report proposed that, Cu^+ acts as the adsorption site for the chemisorption and activation of CO molecules for the CuCe system, but it can hardly catalyze NO elimination and C_3H_6 oxidation [41]. And we also tested the physical mixed sample, and its TWC catalytic ability is not ideal (Fig. S7 in Supporting information). Therefore, it can be proved that the superior TWC activity of the Rh/Cu-CeSn catalyst results from the synergistic effect between Cu and Rh. Additionally, the compared Ce-based catalysts (Rh/Cu-Ce and Rh/CeO_2) were also prepared, among which the supports are replaced by Cu-Ce solid solution and the pure CeO_2 (Figs. S8 and S9 in Supporting information). The result of catalytic performance comparison shows that the promotion effect of Cu modification in Ce-based support is not ideal, and the TWC performance

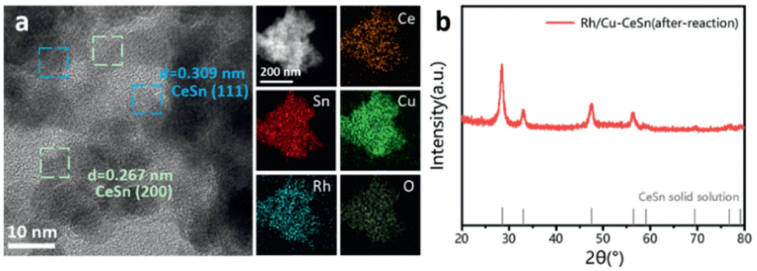

Fig. 5. (a) TEM image of Rh/Cu-CeSn after reaction and the corresponding EDX mapping images. (b) XRD pattern of the Rh/Cu-CeSn after reaction.

is worse than CeSn-based catalysts, reflecting the importance of CeSn solid solution supports (Fig. S10 in Supporting information).

We also optimized the ratio of Ce:Sn:Cu for the Rh/Cu-CeSn catalyst, which are shown in Figs. S11 and S12 (Supporting information). It can be seen that when Ce:Sn increases from 2:1 to 4:1, the catalytic performance presents a volcanic curve distribution, and the catalytic performance is better when the ratio is 3:1. And by adjusting the loading amount of Cu metal, we found that when Ce:Sn:Cu = 6:2:1, the performance of the catalysts is remarkably better than those of Ce:Sn:Cu = 6:2:0.5 and Ce:Sn:Cu = 6:2:2. These comparisons show that the content of Ce, Sn, and Cu is extremely critical for such catalysts, which relates to the formation of solid solutions, the concentration of support oxygen vacancies, and the strength of the synergistic effect among different metals [10,15,42]. Thus, Ce:Sn:Cu = 6:2:1 is considered to be the optimal proportional choice for the Rh/Cu-CeSn catalyst under our test conditions. Eventually, the stability of the Rh/Cu-CeSn catalyst was evaluated by continuous high-temperature reaction at 400 °C for 12 h (Fig. 4d). The conversion of CO, NO, and C_3H_6 of the Rh/Cu-CeSn catalyst decrease slightly and the initial activity retains over 95% after 12 h, which confirms its good stability.

To further verify the stability of the Rh/Cu-CeSn catalyst, its morphology and structure were characterized after the stability test. The TEM image and the corresponding EDX mapping images display that the catalyst still maintains good morphology and Cu, Rh are dispersed well without agglomeration (Fig. 5a). The XRD pattern of the used Rh/Cu-CeSn catalyst shows that there is no clear difference in the structure of the catalysts before and after reaction (Fig. 5b). No diffraction peaks associated with Cu, Rh and other elements appear, representing that the solid solution has no phase separation or metal segregation. And the ICP-OES results of the used Rh/Cu-CeSn catalyst (Table S5) show that the content of Rh element remains almost unchanged after the reaction. Furthermore, the BET specific surface area of the after-reaction Rh/Cu-CeSn is basically the same as that before the reaction, indicating its great stability, which corresponds to the above catalytic test result (Fig. S13 and Table S2 in Supporting information).

In summary, we successfully synthesized a multicomponent catalyst Rh/Cu-CeSn by using Cu metal doping to modify the Ce-based solid solution, which exhibited good TWC catalytic performance: the light-off temperatures for CO, NO, and C_3H_6 conversion are 172 °C, 266 °C, and 193 °C respectively. The experiments and mechanism studies reveal that due to the redox pair Cu^+/Cu^{2+}, the Cu incorporation can effectively inhibit the Rh transition to the oxidation state, maintaining it in a reduced state with high TWC activity, which facilitates the enhancement of catalytic activity and stability greatly. This work represents a feasible strategy for reasonable catalyst design precisely modulating the composite oxide supports during the fabrication of noble metal-based catalysts. We anticipate that the illustrated strategy based on support modification will contribute to upgrading single-atom catalysts for a wide range of catalytic applications.

Declaration of competing interest

The authors declare that they have no known competing financial interests or personal relationships that could have appeared to influence the work reported in this paper.

Acknowledgments

This work was supported by the financial aid from National Science and Technology Major Project of China (No. 2020YFE0204500), National Natural Science Foundation of China (Nos. 22020102003, 22025506 and 11975301) and Youth Innovation Promotion Association of the Chinese Academy of Sciences (No. 2020286).

Supplementary materials

Supplementary material associated with this article can be found, in the online version, at doi:10.1016/j.cclet.2024.109640.

References

[1] J. Lelieveld, J.S. Evans, M. Fnais, et al., Nature 525 (2015) 367–371.
[2] C.K. Lambert, Nat. Catal. 2 (2019) 554–557.
[3] B.J. Finlayson-Pitts, J.N. Pitts Jr., Science 276 (1997) 1045–1051.
[4] S.C. Anenberg, J. Miller, R. Minjares, et al., Nature 545 (2017) 467–471.
[5] Z. Kallas, J.M. Gil, Renew. Energ. 83 (2015) 398–406.
[6] A.K. Neyestanaki, F. Klingstedt, T. Salmi, et al., Fuels 83 (2004) 395–408.
[7] K. Wu, L. Sun, C. Yan, Adv. Energy. Mater. 6 (2016) 1600501.
[8] T. Montini, M. Melchionna, M. Monai, et al., Chem. Rev. 116 (2016) 5987–6041.
[9] S. Wang, M. Sun, M. Huang, et al., Mole Catal. 433 (2017) 162–169.
[10] X. Yao, Y. Xiong, W. Zou, et al., Appl. Catal. B: Environ. 144 (2013) 152–165.
[11] Z. Wang, G. Shen, J. Li, et al., Appl. Catal. B: Environ. 138 (2013) 253–259.
[12] Y. Zeng, Y. Wang, P. Hongmanorom, et al., Chem. Eng. J. 409 (2021) 128242.
[13] R. Kopelent, A. Tereshchenko, A. Guda, et al., ACS Catal. 11 (2021) 9435–9449.
[14] G. Chen, Y. Zhao, G. Fu, et al., Science 344 (2014) 495–499.
[15] M.F. Camellone, S. Fabris, J. Ning, et al., Nat. Catal. 2 (2019) 334–341.
[16] C. Copéret, A.C. Vives, M.P. Conley, et al., Chem. Rev. 116 (2016) 323–421.
[17] K. An, S. Alayoglu, N. Musselwhite, et al., J. Am. Chem. Soc. 135 (2013) 16689–16696.
[18] M. Kuhn, S.R. Bishop, J.L.M. Rupp, et al., Acta. Mater. 61 (2013) 4277–4288.
[19] A. Gupta, U.V. Waghmare, M.S. Hegde, et al., Chem. Mater. 22 (2010) 5184–5198.
[20] J.L. Ayastuy, A. Iglesias-González, M.A. Gutiérrez-Ortiz, Chem. Eng. J. 244 (2014) 372–381.
[21] D.R. Sellick, A. Aranda, T. García, et al., Appl. Catal. B: Environ. 132 (2013) 98–106.
[22] J.L. Ayastuy, A. Gurbani, M.P. González-Marcos, et al., Int. J. Hydrogen Energy. 37 (2012) 1993–2006.
[23] A. Iglesias-González, J.L. Ayastuy, M.P. González-Marcos, et al., Int. J. Hydrogen Energy 39 (2014) 5213–5224.
[24] G. Avgouropoulos, T. Ioannides, H. Matralis, Appl. Catal. B: Environ. 56 (2005) 87–93.
[25] M. Liu, R. Yan, Y. Wang, et al., ChemistrySelect 7 (2022) e202100433.
[26] G. Aguila, S. Guerrero, P. Baeza, et al., Mater. Chem. Phys. 223 (2019) 666–675.
[27] M.J. Kim, H.J. Kim, S.J. Lee, et al., Catal. Comm. 130 (2019) 105764.
[28] H. Asakura, S. Hosokawa, T. Ina, et al., J. Am. Chem. Soc. 140 (2018) 176–184.
[29] Y. Su, G. Xia, Y. Qin, et al., Chem. Sci. 12 (2021) 8260–8267.
[30] J. Chen, S. Xiong, H. Liu, et al., Nat. Comm. 14 (2023) 3477.
[31] Y. Cao, R. Ran, X. Wu, et al., Catal. Today 281 (2017) 490–499.
[32] J. Wan, J. Lin, X. Guo, et al., Chem. Eng. J. 368 (2019) 719–729.

[33] A. Schön, J.P. Dacquin, P. Granger, et al., Appl. Catal. B: Environ. 223 (2018) 167–176.
[34] J. Li, Z. Liu, D.A. Cullen, et al., ACS Catal. 9 (2019) 11088–11103.
[35] Y. Deng, P. Tian, S. Liu, et al., J. Hazard. Mater. 426 (2021) 127793.
[36] J.C. Matsubu, V.N. Yang, P. Christopher, J. Am. Chem. Soc. 137 (2015) 3076–3084.
[37] R. Lan, T. Li, D. Matsumura, et al., Angew. Chem. Int. Ed. 55 (2016) 16054–16058.
[38] K. Khivantsev, C.G. Vargas, J. Tian, et al., Angew. Chem. Int. Ed. 60 (2021) 391–398.
[39] L. Dong, Y. Tang, B. Li, et al., Appl. Catal. B: Environ. 180 (2016) 451–462.
[40] B. Huang, H. Kobayashi, T. Yamamot, et al., Angew. Chem. Int. Ed. 58 (2018) 2230–2235.
[41] J. Lu, J. Wang, Q. Zou, et al., ACS Catal. 9 (2019) 2177–2195.
[42] L. Kang, B. Wang, Q. Bing, et al., Nat. Comm. 11 (2020) 4008.